Electronic structure of $La_{1.48}Nd_{0.4}Sr_{0.12}CuO_4$ probed by high- and low-energy angle-resolved photoelectron spectroscopy

T. Claesson,[1] M. Månsson,[1,2] A. Önsten,[1] M. Shi,[3] Y. Sassa,[2] S. Pailhés,[2] J. Chang,[2] A. Bendounan,[4] L. Patthey,[3] J. Mesot,[5] T. Muro,[6] T. Matsushita,[6] T. Kinoshita,[6] T. Nakamura,[6] N. Momono,[7] M. Oda,[7] M. Ido,[7] and O. Tjernberg[1,*]

[1]*Materials Physics, KTH Royal Institute of Technology, Electrum 229, S-164 40 Kista, Sweden*

[2]*Laboratory for Neutron Scattering, ETH Zürich and Paul Scherrer Institut, CH-5232 Villigen PSI, Switzerland*

[3]*Swiss Light Source, Paul Scherrer Institut, CH-5232 Villigen PSI, Switzerland*

[4]*Synchrotron SOLEIL, L'Orme des Merisiers, Saint-Aubin, 91192 Gif-sur-Yvette Cedex, France*

[5]*Paul Scherrer Institute, ETH Zürich, EPF Lausanne, CH-5232 Villigen PSI, Switzerland*

[6]*Japan Synchrotron Radiation Research Institute, SPring-8, Sayo, Hyogo 679-5198, Japan*

[7]*Department of Physics, Hokkaido University, Sapporo 060-0810, Japan*

(Received 2 December 2008; revised manuscript received 4 August 2009; published 4 September 2009)

We present angle-resolved photoelectron spectroscopy data probing the electronic structure of the Nd-substituted high-T_c cuprate $La_{1.48}Nd_{0.4}Sr_{0.12}CuO_4$. Data have been acquired at low and high photon energies, $h\nu$=55 and 500 eV, respectively. The two extracted Fermi surfaces show significant differences. The differences can be attributed to either the change in probing depth suggesting dissimilarity of the intrinsic electronic structure between surface and bulk regions, or a considerable c-axis dispersion signaling a strong interlayer coupling. At both photon energies, considerable spectral weight is observed at all points along the Fermi surface and the intensity distribution as well as Fermi-surface shape observed at low as well as high photon energy is markedly different from what has been previously reported for $La_{1.28}Nd_{0.6}Sr_{0.12}CuO_4$ by Zhou *et al.* [Science **286**, 268 (1999)].

DOI: 10.1103/PhysRevB.80.094503 PACS number(s): 74.25.Jb, 71.18.+y, 74.72.−h, 79.60.−i

I. INTRODUCTION

High-temperature superconductivity (HTSC) has remained one of the major intellectual challenges for condensed-matter physicists during more than twenty years.[1,2] One of the most important experimental tools available to investigate the electronic properties of HTSC has been angle-resolved photoelectron spectroscopy (ARPES). This technique can directly probe the spectral function $A(\vec{k},\omega)$ and, undoubtedly, there is no disagreement regarding the huge impact ARPES has had for the understanding of HTSC. However, some skepticism has been raised concerning the significance of studying a bulk phenomena by means of a surface-sensitive technique.[3] These constraints have currently been partly overcome through technical development giving access to more bulk-sensitive measurements.[4,5] The importance of obtaining an electronic structure representative of the bulk became even more evident with the recent observation of quantum oscillations in underdoped $YBa_2Cu_3O_{7-\delta}$ (YBCO) samples.[6] This suggested that the reduction of the Fermi surface (FS) into disconnected Fermi arcs for underdoped cuprates might not necessarily be connected to the existence of a pseudogap[7,8] but rather to a Fermi-surface reconstruction into hole and/or electron pockets.[6,9,10] Contrary, even though attempts have been made, high-quality ARPES data[11] show no direct evidence of such Fermi-surface reconstruction/pockets. This raises the question how to adequately connect bulk-sensitive quantum oscillation measurements made in high magnetic fields (pseudogap phase) with ARPES data in the superconducting state.[11]

The vast majority of ARPES studies on cuprate high-T_c systems have been performed in a small range of relatively low photon energies, 20–100 eV. At these energies ARPES experiments suffer from a number of limitations and a certain amount of caution is necessary in the interpretation of such data. Particular attention should be paid to the fact that the typical probing depth in this energy range is approximately 5 Å.[12] The limited probing depth can pose a problem since a significant amount of the measured intensity comes from other parts of the crystal structure than the deep lying CuO_2 planes believed to be responsible for the mechanism of HTSC. Further, for low photon energies, attention should also be paid to the relatively large angular ranges that can result in considerable variations in the optical matrix elements. These and other difficulties are to some extent overcome by carrying out ARPES measurements at higher photon energies in the soft x-ray region where the probing depth is larger ($\lambda_e \approx 10-15$ Å) (Ref. 12) and the angular ranges smaller. However, in this energy range other drawbacks appear, for instance, the cross section for the photoelectric effect is much lower and the obtainable energy and angular resolutions are worse, as compared to the 20–100 eV photon energy range. Not until recently has the experimental progress permitted successful studies of the electronic structure using ARPES at soft x-ray photon energies.[4,13–15] Given the benefits and drawbacks of ARPES performed at low and soft x-ray photon energies, respectively, the combination of ARPES studies carried out in both energy ranges would provide a much more complete picture of the electronic structure in systems such as the strongly correlated cuprate superconductors.

One of the most studied cuprate HTSC systems is the $La_2CuO_{4+\delta}$ system, which by the addition of Sr is hole doped to give $La_{2-x}Sr_xCuO_4$ (LSCO). The possibility to grow high-quality single crystalline samples over a wide Sr doping

range has enabled a large amount of experimental studies devoted to its electronic structure. Contributions have come from several diverse experimental fields, for instance neutron scattering,[16] x-ray scattering[17] and ARPES.[18] Two of the investigated properties are the suppression of superconductivity in LSCO near $x=0.12$ and the existence of dynamic and static one-dimensional charge ordering (sometimes called stripes) in LSCO and the Nd-substituted $La_{2-x-y}Nd_ySr_xCuO_4$ (Nd-LSCO).

Here we report an ARPES study performed on the $La_{2-x-y}Nd_ySr_xCuO_4$ $(x=0.12, y=0.4)$ system at two different photon energies, $h\nu=55$ eV and $h\nu=500$ eV. The low photon energy data set permits a detailed analysis of the near Fermi edge dispersion along the entire Fermi surface from the *d*-wave gap node direction to the antinode direction. On the other hand, the high photon energy data give access to the electronic structure at a larger probing depth. In turn, this enables a comparison to the low-energy data regarding features such as the shape and volume of the Fermi surface and the distribution of spectral intensity along it.

II. EXPERIMENTAL DETAILS

The single crystalline $La_{1.48}Nd_{0.4}Sr_{0.12}CuO_4$ (Nd-LSCO) sample was grown by the traveling solvent floating zone method[19] and had a $T_c=7$ K. The high quality of the sample has been confirmed by neutron-scattering measurements[20,21] performed on this particular batch. The samples were cleaved *in situ* under ultrahigh-vacuum conditions (base pressure $<2\times10^{-10}$ mbar) using a specially designed cleaver[22] (low-energy data) and so-called postcleaving (high-energy data), respectively. ARPES measurements were performed at two different synchrotron-radiation facilities: (1) Swiss Light Source (SLS) synchrotron-radiation facility using the Surface and Interface Spectroscopy beam line X09LA-HRPES (Ref. 23) and (2) SPring-8 synchrotron-radiation facility using the BL25SU beam line.[24] At the former beam line we have performed low photon energy ($h\nu=55$ eV) ARPES with $\Delta E=20$ meV and $T=20$ K using circularly polarized light. At the latter beam line we have performed high photon energy ($h\nu=500$ eV) ARPES measurements with $\Delta E=100$ meV at $T=20$ K, also using circularly polarized light. In both cases, the angle of incidence was 45° and the angle of emission close to normal (first and second zone). Both ARPES end stations are equipped with Gammadata Scienta angle-resolving electron analyzers, the SLS end station had the SES-2002 model while the SPring- 8 end station had the SES-200 model. The angular resolution along the analyzer slit was in both data sets on the order of ±0.1°, corresponding to momentum resolutions of 0.006 and 0.020 Å^{-1}. In the direction perpendicular to the analyzer slit, the momentum resolutions were on the order of 0.019 and 0.030 Å^{-1} at low and high photon energies, respectively. In both experimental setups, off-normal incidence was used in concert with circularly polarized light as to minimize any symmetry related suppression of the optical matrix elements.

III. RESULTS AND DISCUSSION

Figure 1(a) presents a typical ARPES spectrum acquired at $h\nu=55$ eV, where the spectral intensity is shown as a function of binding energy and electron momentum. A well-defined dispersive valence-band feature crosses the Fermi level close to $k=0.1$ Å^{-1}. The momentum-space orientation of this particular cut is close to the *d*-wave gap node direction, as displayed in the inset of (b). White dashed lines indicate the energy position of the Fermi level (E_F) and the momentum location of the energy distribution curve (EDC) displayed in (b). The Fermi level has been determined by a Fermi function fit to photoemission data recorded from polycrystalline copper of the sample holder. The EDC at the momentum position where the valence band crosses the Fermi level shows a pronounced peak structure with a clear Fermi cutoff. This experimental finding contrasts with results from $La_{1.28}Nd_{0.6}Sr_{0.12}CuO_4$ obtained by Zhou *et al.*[18] At the same level of Sr doping ($x=0.12$) but with a different amount of Nd substitution these authors found no dispersing feature in the Γ-(π,π) direction, where the cuprates usually show the most pronounced dispersion with well-defined quasiparticle peaks.

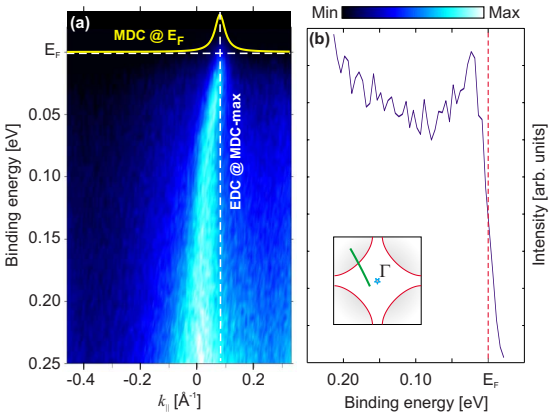

FIG. 1. (Color online) (a) ARPES spectrum acquired at $h\nu=55$ eV displayed as a color coded intensity map. Spectral intensity is displayed as a function of electron momentum and binding energy. The momentum-space orientation of this cut is displayed by the inset in (b). White dashed lines indicate the Fermi level (E_F) and the momentum position of the energy distribution curve shown in (b). Solid (yellow) line represent the momentum distribution curve at E_F. (b) Energy distribution curve acquired at the momentum indicated in (a). The solid red line in the inset is a schematic Fermi-surface contour serving as a guide to the eye.

Figure 2(a) shows a color coded intensity map of the distribution of integrated spectral weight around the Fermi-surface contour for the 55 eV data set. The intensity map was obtained by subtracting a linear background from each MDC and then integrating the spectral intensity over an energy window ranging from 10 meV below to 5 meV above the Fermi level. The acquired ARPES data have been folded into one quadrant of the two-dimensional Brillouin zone and symmetrized with respect to the Γ-(π,π) line and finally repeated to cover the complete zone. Blue circular dots in Fig. 2(b) display the Fermi surface at 55 eV determined from Lorentzian fits of momentum distribution curves (MDC) at E_F [see, e.g., yellow line in Fig. 1(a)]. The red dashed line in (b) indicates a Fermi-surface contour determined from the same tight-binding expression for the dispersion in a CuO_2 plaquette as in Ref. 26. The respective tight-binding param-

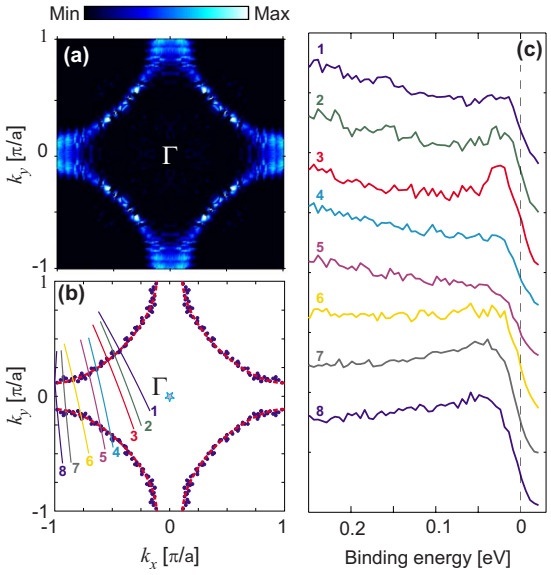

FIG. 2. (Color online) (a) Near Fermi-level Nd-LSCO spectral intensity for the 55 eV data displayed as a color coded momentum-space map. The valence-band intensity was integrated over an energy window ranging from 10 below to 5 meV above the Fermi level. (b) Fermi-level crossings of the valence band as determined from functional fits of momentum distribution curves at E_F to a Lorenztian function. The red dashed line indicates the Fermi surface resulting from a tight-binding expression for a CuO_2 plane. Tight-binding parameters[25] are chosen so as to obtain a good fit to our data. (c) A series of angle-resolved energy distribution curves acquired at different positions along the Fermi-surface contour. The shown EDCs are acquired at the momenta where the corresponding numbered angular cut in (b) crosses the Fermi surface.

eter values are chosen to achieve a good fit with our experimental data.[25] Figure 2(c) displays a series of angle-resolved EDCs acquired at different momenta between the nodal and antinodal directions. The shown EDCs are acquired at the momentum where the corresponding numbered angular cut in (b) crosses the Fermi surface.

When moving along the Fermi surface from the nodal direction toward the $(\pi,0)$ antinodal point, the EDCs show some evolution in terms of spectral shape. The near Fermi edge peak structure is most sharp in EDC number 3, slightly suppressed in 4–6 and finally starts to gain weight and gets more well defined again close to the antinode in 7 and 8. These peaks are, however, much broader than those observed for $La_{2-x}Sr_xCuO_4$ $(x=0.145,0.17)$ in the superconducting state[26–28] and hence it is difficult to characterize them as quasiparticle peaks in a strict sense. Still, it is possible to identify a more or less sharp peak in angle-resolved EDCs for all momenta around the entire Fermi-surface contour. This behavior contrasts to the results of Zhou *et al.*,[18] who did not find any EDCs with sharp peak structure along the entire Fermi-surface contour, although some dispersion was clearly present in certain regions of the Brillouin zone.

Returning to the shape of the Fermi surface, one observes that the Fermi-surface contour is centered around the Γ point and has a volume reasonably consistent with the value $1-x$ given by the Luttinger theorem.[29] With a filling level of 0.86 ± 0.05 the Luttinger theorem gives a doping level $x=0.14$. Considering the limits given by experimental uncertainty, this value agrees well with the nominal doping level of our sample $(x=0.12)$. The shape of this Fermi-surface contour and the distribution of intensity around it are both significantly different from the ARPES results from $La_{1.28}Nd_{0.6}Sr_{0.12}CuO_4$ (Ref. 18) where the Fermi-level intensity was confined to straight patches located in a small momentum-space region centered on the $(\pi,0)$ antinodal point. The present data also display a region of strong intensity around the $(\pi,0)$ point. However its shape is different from that in Ref. 18 in that the boundary of spectral weight confinement is straight, while it is curved in the present data. Near $(\pi,0)$ the locus of maximum intensity in Fig. 2(a) closely follows the red dotted curve resulting from a tight-binding expression in (b). This behavior also contrasts to that in the data of Zhou *et al.*, where the intensity reaches its maximum value in a small region of almost circular shape centered on the $(\pi,0)$ point.

Except for the antinodal area of the Brillouin zone, Zhou *et al.*[18] found only very weak spectral intensity. Especially in the vicinity of the $(\pi/2,\pi/2)$ point the suppression of intensity was almost complete, giving a very poorly defined Fermi surface. A later ARPES study on $La_{1.4-x}Nd_{0.6}Sr_xCuO_4$ $(x=0.10,0.15)$ (Ref. 30) indicated the presence of spectral weight in this region, though still not with a similar intensity distribution as in the present data set. Our ARPES data when integrated over a 15 meV wide energy window result in evident spectral intensity along the entire Fermi surface, also in the vicinity of the $(\pi/2,\pi/2)$ point. This smoother intensity distribution is more consistent with a weak charge-density modulation whereas a strong suppression of spectral weight in the *d*-wave node direction would point to a strong charge modulation. Even though the amount of Nd substitution differs in our case (0.4) as compared to Ref. 18 (0.6), the difference between the two data sets is surprising. In the present data set, which is collected with circularly polarized light at 45° incidence, the electric-field vector is of similar magnitude along all crystal directions and no matrix element suppression is expected on geometrical grounds. This is consistent with the even intensity distribution that we observe. In comparison, the suppression of intensity at the $(\pi/2,\pi/2)$ point observed by Zhou *et al.* leads the thought to a matrix element effect.

Furthermore, it is interesting to compare the shape of the near Fermi edge distribution of spectral weight from ARPES measurements with results from calculations. LDA calculations on the $La_{2-x}Sr_xCuO_4$ system[31,32] have indicated a notable valence-band dispersion with respect to the out-of-plane component of electron momentum, k_z. Xu *et al.*[31] presented such LDA results and show the Fermi-surface topology for $k_z=0$ and $k_z=\pi/c$. Our 55 eV ARPES results show a spectral weight distribution of reasonably similar shape as compared to the calculated results for $k_z=0$ where the LDA Fermi-surface contour to a large extent runs perpendicular to the nodal direction, c.f. the red dashed curve in Fig. 2(b) of the present study.

Turning now to the high-energy results, several aspects speak for the importance of bulk-sensitive photoemission measurements on the cuprate HTSC. Cleaving of an Nd-LSCO single crystal will always result in a sample with dif-

ferences in electronic structure between the outermost surface layer(s) and the deeper lying bulk material. Such differences can definitely induce modifications in the electronic structure as probed by ARPES.[4] Moreover, the layered high-T_c cuprate compounds have a large unit cell with one or several CuO_2 planes, from where the fundamental mechanisms of superconductivity are believed to originate. Virtually all ARPES measurements on high-T_c systems have been interpreted as reflecting the electronic structure of these CuO_2 planes. This assumption is not necessarily true. For instance, cleaving of a single-crystal cuprate sample could easily result in a sample surface with the outermost CuO_2 plane positioned at a depth of several Ångströms beneath the cleaved surface. The commonly used range of photon energies for ARPES measurements on these systems is 20–100 eV, which makes the measurement very surface sensitive[12] and implies that the signal from the CuO planes can very well be masked or distorted by the outermost planes. There have been observations of a strong inelastic and photon energy dependent scattering in Sr and Ca core-level photoemission data from another compound in the cuprate family, namely $Bi_2Sr_2CaCu_2O_{8+\delta}$.[33] Scattering of this kind gives a reduced mean-free path for the photoemitted electrons. For emission from a deeply lying CuO_2 plane this type of scattering could reduce the mean-free path to such a degree that these electrons only would contribute a small part of the total photoemission signal. The influence of such effects on photoemission data can be somewhat reduced by performing experiments using photon energies in the soft x-ray region. Moreover, the limited angular range and the higher kinetic energies resulting from the use of soft x-rays has the added advantages of smaller variations in the optical matrix elements and a photoelectron that is more effectively decoupled from the rest of the system. The latter justifies the interpretation of the intensity as being proportional to the spectral function for the system.

Figure 3(a) displays an ARPES spectrum from Nd-LSCO acquired at a photon energy of 500 eV. One can clearly discern two distinct dispersive valence-band features crossing the Fermi level in the momentum region $k=0.4$ to 1.0 Å^{-1}. Weaker signs of another dispersive feature can also be noted near $k=-1.0$ Å^{-1}. The presence of three distinct crossings is even more evident when studying the MDC at E_F shown in Fig. 3(c). Even though the spectra of Figs. 1(a) and 3(a) are collected using the same analyzer acceptance angles, a much larger part of momentum space is covered in the latter, due to the use of the higher photon energy. The momentum-space orientation of this particular cut is displayed in Fig. 3(b).

The combination of an inferior energy resolution and a lower count rate for photoemission experiments in the soft x-ray energy region makes it difficult to perform a detailed analysis in terms of EDC peak dispersion, as was done for the low-energy data set. However, the near Fermi edge distribution of spectral weight is readily analyzed and can also be compared to the low-energy results. The two data sets (low and high energy) were obtained with energy resolutions of 20 and 97 meV, respectively. To be able to compare the two data sets, we have simulated the effect of a different energy and angular resolution in the low-energy data in the following way. The low-energy ARPES spectra have been

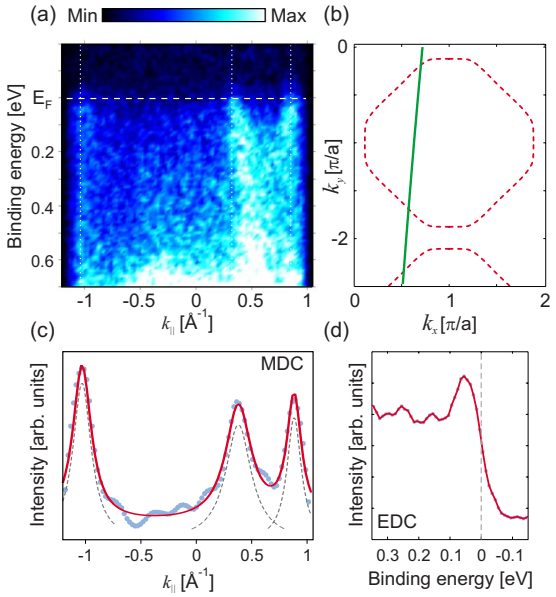

FIG. 3. (Color online) (a) ARPES spectrum acquired at $h\nu=500$ eV displayed as a color-coded intensity map. Photoemitted intensity is displayed as a function of binding energy and electron momentum. The dashed white line indicates the Fermi level (E_F). Two evident and one less apparent Fermi-level crossings are shown, with the momentum position indicated by three vertical dotted lines. (b) Momentum space location of the angular cut [solid (green) line] displayed in (a). The dashed (red) line is a schematic Fermi-surface contour serving as a guide to the eyes. (c) MDC at E_F clearly showing the three crossings. Thick solid (red) line represents a Lorentzian fit to the data with three individual peaks (dashed gray line). (d) EDC acquired at k_F.

energy and momentum broadened by convolution with Gaussian functions so that the total broadening (instrument plus convolution) is equal to the instrumental broadening of the high-energy data (97 meV and 0.020 Å^{-1}). Figure 4 displays color coded maps of spectral intensity integrated over an energy window ranging from 40 below to 30 meV above the Fermi level for the broadened low-energy (55 eV) data and the high-energy (500 eV) data. The spectral intensity displayed in this figure has been symmetrized to fill the complete Brillouin zone in the same way as for Fig. 2(a).

As the Gaussian broadened intensity map of Fig. 4(a) is compared to that based on the untreated ARPES spectra in Fig. 2(a), one notices that the two figures are very similar as far as both shape and distribution of spectral intensity are concerned. The only noticeable influence from the modified energy integration window and the broadening is a slight smearing and redistribution of intensity at the antinode.

A more interesting comparison is that between the two intensity maps in Fig. 4. At high energy (b), spectral weight is present along the entire contour from the nodal to the antinodal direction. This behavior is similar to the 55 eV data and the high-energy contour encloses a region, whose volume is reasonably consistent with the Luttinger value $1-x$. A filling level of 0.84 ± 0.05 corresponds to a doping value x of 0.16 which is higher than the nominal doping level of $x=0.12$ but still within the uncertainty limit of our data. The energy broadened 55 eV data in the same way result in a

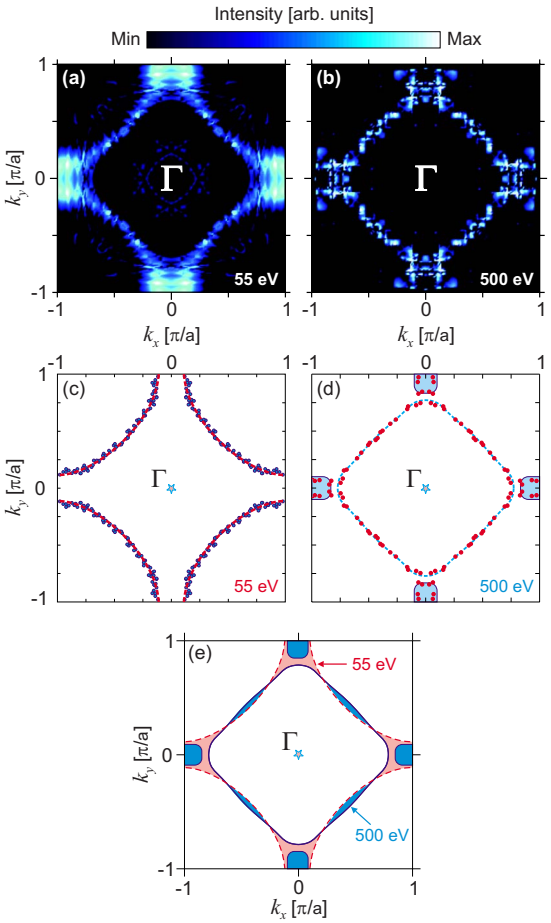

FIG. 4. (Color online) Color coded momentum-space maps of near Fermi-level spectral weight derived from ARPES data acquired at (a) $h\nu$=55 (b) and 500 eV. In order to simulate the effect of a different energy and momentum resolution, the 55 eV spectrum [from Fig. 2(a)] has been broadened by convolution with Gaussian functions. The ARPES intensity is integrated over an energy window from 40 below to 30 meV above the Fermi level in both (a) and (b). (c) Fermi-level crossings of the valence band as determined from functional fits of momentum distribution curves at E_F to a Lorenztian function [same as Fig. 2(b)]. (d) Same as (c) but for the 500 eV data. Note that the dashed (blue) line is a simple guide to the eye. (e) Schematic figure showing the clear difference in FS shape between high and low photon energy. Light (pink) and dark (blue) shaded areas show where the 55 eV FS [dashed (red) line] and the 500 eV FS [solid (blue) line] deviate from each other.

filling level of 0.86 ± 0.04, corresponding to an actual doping level of 0.14, as before and confirming the limited effect of the added broadening. The difference in measured doping level between 55 and 500 eV could indicate a difference in doping between the surface and bulk region or a possible k-perpendicular dependence, but it is difficult to draw such a conclusion in view of the experimental uncertainties involved.

Regarding the shape and distribution of spectral weight along the Fermi surface there are notable differences between the low- and high-energy data. In Fig. 4(a) one notices the relatively large concentration of spectral intensity in a small area around the antinodal point, while the intensity is lower in other parts along the contour. The high-energy data of Fig. 4(b) has a more uniform intensity distribution with the antinode region at about the same intensity level as other parts of the contour.

Also shown in Fig. 4 is the Fermi surface as determined by Lorentzian fits to the momentum distribution curves at E_F [c.f. Fig. 3(c)]. Such fits give a more accurate determination of the Fermi-surface shape than the simple intensity integration around E_F. In the present case, the Fermi-surface shapes given by the intensity integration and by fitting the MDCs give a very similar picture. Comparing the high and low-energy data, it is clear that there is a substantial difference between the more surface-sensitive and the more bulk-sensitive data [see Fig. 4(c)]. The low-energy intensity in (c) approximately follows a contour whose center of curvature is located at the (π,π) point. In contrast, the large segment in (d) is almost square and appears to be closed around the Γ point. One also notices that the high-energy Fermi-surface contour seems to be composed of different segments. Besides the large segment already mentioned, one can also imagine a small pocket centered at $(\pi,0)$. In view of the limited number of k points in Fig. 4(d) one should be cautious about jumping to conclusions; but in view of the experimental evidence for small Fermi-surface pockets in underdoped $YBa_2Cu_3O_{6.5}$ (Ref. 6) it is tempting to speculate along those lines. Continuing on that track, it is tempting to re-evaluate the increased intensity observed at $(\pi,0)$ in Fig. 4(a) and Ref. 18 as originating from pockets.

The observed differences in the Fermi-surface shape are either related to the difference in probing depth between low and high kinetic energies or the result of k_z dispersion. Since, to our knowledge, there have been no observations of a substantial k_z dependence in the low photon energy range (6–60 eV) in other high-T_c systems we find it plausible that the k_z dependence is weak also in $La_{1.48}Nd_{0.4}Sr_{0.12}CuO_4$. As a result, the observed differences can most likely be attributed to differences between the bulk and surface electronic structure. This demonstrates that caution is necessary when interpreting low-energy photoemission data as indicative of bulk properties even in quasi two-dimensional systems such as the cuprates. As a matter of fact, comparable behavior has already been observed in related systems. A similar result with a modified Fermi-surface shape was previously observed in soft x-ray ARPES data from $Nd_{2-x}Ce_xCuO_4$.[4] Highly bulk-sensitive hard x-ray photoelectron spectroscopy (XPS) data on $La_{2-x}Sr_xCuO_4$ and $Nd_{2-x}Ce_xCuO_4$ (Ref. 34) have also indicated a modified electronic structure down to probing depths of several nanometers.

As was done for the 55 eV data, one can also compare the shape of the high-energy contour from our ARPES measurements with results from LDA calculations on the $La_{2-x}Sr_xCuO_4$ system.[31] In these theoretical results, a notable dispersion of the Fermi-surface contour with respect to the out-of-plane component of electron momentum, k_z, is observed. Based on this theoretical prediction it is hence possible to interpret the deviations in Fermi-surface shape observed between the low- and high-energy data as partly due to probing of a different k_z value. That such a k_z-dependence was not found in low photon energy studies could be explained by the inferior k_z-resolution achieved at lower photon energies.[35]

IV. CONCLUSIONS

To conclude, the present ARPES study of the Nd-LSCO system has demonstrated the presence of spectral weight along the entire Fermi-surface contour. No regions with dramatically suppressed spectral intensity are found and hence our data would be more consistent with the presence of weak charge modulations. However, based on this observation it is difficult to draw any distinct conclusions regarding the influence of so-called stripes in this compound. On the other hand, data at low and high photon energies show significant differences in the near Fermi edge spectral characteristics for high versus low photon energies. At high energy, the spectral weight seems to be more evenly distributed over the entire Fermi-surface contour, not showing particularly elevated intensity close to the $(\pi,0)$ point as is observed in the 55 eV data. Most noteworthy is perhaps a distinct change in Fermi-surface shape between the 55 and 500 eV data sets. In going from low to high photon energy, the shape goes from being curved around the (π,π) point to an almost square Fermi-surface centered around Γ with the possibility of pockets at $(\pi,0)$. The observed differences can attributed to the increase in photoelectron probing depth, *k*-perpendicular dispersion or a combination of both. In the first case, the present results would indicate a substantial surface influence on the electronic structure and in the second a considerable interlayer coupling. In any case, the present results underline the importance of performing further high-energy studies on cuprates in order to capture their true bulk behavior.

ACKNOWLEDGMENTS

This research has been supported by the Swedish Research Council, the Göran Gustafsson Foundation, the Knut and Alice Wallenberg Foundation, the Foundation BLANCEFLOR Boncompagni-Ludovisi née Bildt, the Foundation for Strategic Research (SSF), the Swiss National Science Foundation (through NCCR, MaNEP, and Grant No. 200020-105151), the European Union, and the Japan Synchrotron Radiation Research Institute (JASRI) through a "Budding Researchers Support Proposal" (Proposal No. 2006B1020).

*oscar@kth.se

[1] J. G. Bednorz and K. A. Müller, Z. Phys. B **64**, 189 (1986).
[2] J. Zaanen, Nat. Phys. **2**, 138 (2006).
[3] M. P. Seah and W. A. Denc, Surf. Interface Anal. **1**, 2 (1979).
[4] T. Claesson, M. Månsson, C. Dallera, F. Venturini, C. De Nadaï, N. B. Brookes, and O. Tjernberg, Phys. Rev. Lett. **93**, 136402 (2004).
[5] M. Okawa *et al.*, Phys. Rev. B **79**, 144528 (2009).
[6] N. Doiron-Leyraud, C. Proust, D. LeBoeuf, J. Levallois, J.-B. Bonnemaison, R. Liang, D. A. Bonn, W. N. Hardy, and L. Taillefer, Nature (London) **447**, 565 (2007).
[7] A. Kanigel *et al.*, Nat. Phys. **2**, 447 (2006).
[8] K. M. Shen *et al.*, Science **307**, 901 (2005).
[9] D. LeBoeuf *et al.*, Nature (London) **450**, 533 (2007).
[10] C. Jaudet *et al.*, Phys. Rev. Lett. **100**, 187005 (2008).
[11] M. A. Hossain *et al.*, Nat. Phys. **4**, 527 (2008).
[12] W. S. M. Werner, C. Tomastik, T. Cabela, G. Richter, and H. Störi, Surf. Sci. **470**, L123 (2000).
[13] A. Önsten, M. Månsson, T. Claesson, T. Muro, T. Matsushita, T. Nakamura, T. Kinoshita, U. O. Karlsson, and O. Tjernberg, Phys. Rev. B **76**, 115127 (2007).
[14] S.-I. Fujimori, Y. Saitoh, T. Okane, A. Fujimori, H. Yamagami, Y. Haga, E. Yamamoto, and Y. Ōnuki, Nat. Phys. **3**, 618 (2007).
[15] M. Månsson, T. Claesson, M. Finazzi, C. Dallera, N. B. Brookes, and O. Tjernberg, Phys. Rev. Lett. **101**, 226404 (2008).
[16] N. B. Christensen, H. M. Rønnow, J. Mesot, R. A. Ewings, N. Momono, M. Oda, M. Ido, M. Enderle, D. F. McMorrow, and A. T. Boothroyd, Phys. Rev. Lett. **98**, 197003 (2007).
[17] M. v. Zimmermann *et al.*, Europhys. Lett. **41**, 629 (1998).
[18] X. J. Zhou, P. Bogdanov, S. A. Kellar, T. Noda, H. Eisaki, S. Uchida, Z. Hussain, and Z.-X. Shen, Science **286**, 268 (1999).
[19] T. Nakano, N. Momono, M. Oda, and M. Ido, J. Phys. Soc. Jpn. **67**, 2622 (1998).
[20] J. Chang, C. Niedermayer, R. Gilardi, N. B. Christensen, H. M. Rønnow, D. F. McMorrow, M. Ay, J. Stahn, O. Sobolev, A. Hiess, S. Pailhes, C. Baines, N. Momono, M. Oda, M. Ido, and J. Mesot, Phys. Rev. B **78**, 104525 (2008).
[21] J. Chang, N. B. Christensen, C. Niedermayer, K. Lefmann, H. M. Rønnow, D. F. McMorrow, A. Schneidewind, P. Link, A. Hiess, M. Boehm, R. Mottl, S. Pailhes, N. Momono, M. Oda, M. Ido, and J. Mesot, Phys. Rev. Lett. **102**, 177006 (2009).
[22] M. Månsson *et al.*, Rev. Sci. Instrum. **78**, 076103 (2007).
[23] U. Flechsig, L. Patthey, and T. Schmidt, in *Synchrotron Radiation Instrumentation*, edited by T. Warwick, J. Stöhr, H. A. Padmore, and J. Arthur, AIP Conf. Proc. No. 705 (AIP, New York, 2004), p. 316.
[24] Y. Saitoh *et al.*, Rev. Sci. Instrum. **71**, 3254 (2000).
[25] The tight-binding parameter values used in the expression that produces the contour in Fig. 2(b) are: $\mu=0.1914$, $t=0.25$, $t'=-0.0370$, and $t''=0.0185$.
[26] J. Chang *et al.*, Phys. Rev. B **75**, 224508 (2007).
[27] M. Shi, J. Chang, S. Pailhés, M. R. Norman, J. C. Campuzano, M. Månsson, T. Claesson, O. Tjernberg, A. Bendounan, L. Patthey, N. Momono, M. Oda, M. Ido, C. Mudry, and J. Mesot, Phys. Rev. Lett. **101**, 047002 (2008).
[28] J. Chang, Y. Sassa, S. Guerrero, M. Månsson, M. Shi, S. Pailhés, A. Bendounan, R. Mottl, T. Claesson, O. Tjernberg, L. Patthey, M. Ido, M. Oda, N. Momono, C. Mudry, and J. Mesot, New J. Phys. **10**, 103016 (2008).
[29] J. M. Luttinger, Phys. Rev. **119**, 1153 (1960).
[30] X. J. Zhou *et al.*, Phys. Rev. Lett. **86**, 5578 (2001).
[31] J.-H. Xu, T. J. Watson-Young, J. Yu, and A. J. Freeman, Phys. Lett. A **120**, 489 (1987).
[32] S. Sahrakorpi, M. Lindroos, R. S. Markiewicz, and A. Bansil, Phys. Rev. Lett. **95**, 157601 (2005).
[33] A. A. Zakharov, I. Lindau, and R. Yoshizaki, Physica C **398**, 49 (2003).
[34] M. Taguchi *et al.*, Phys. Rev. Lett. **95**, 177002 (2005).
[35] The escape depth of the photoemitted electron is directly related to the momentum-space resolution in the surface-normal direction (z) through the Heisenberg principle $\Delta k_z \approx 1/\lambda_e$.